








Prioritizing commercial thinning: quantification of growth and competition with high-density drone laser scanning

Liam A.K. Irwin ^{1,*}, Nicholas C. Coops ¹, José Riofrío ¹, Samuel G. Grubinger ¹, Ignacio Barbeito ¹, Alexis Achim ², Dominik Roeser ¹

¹Department of Forest Resources Management, University of British Columbia, 2424 Main Mall, Vancouver, British Columbia V6T1Z4, Canada

²Department of Wood and Forest Sciences, Université Laval, 2425 rue de la Terrasse, Québec G1V 0A6, Canada

*Corresponding author. Department of Forest Resources Management, University of British Columbia, 2424 Main Mall, Vancouver, British Columbia V6T1Z4, Canada. E-mail: liamakirwin@gmail.com

Abstract

Laser scanning sensors mounted on drones enable on-demand quantification of forest structure through the collection of high-density point clouds (500+ points m⁻²). These point clouds facilitate the detection of individual trees enabling the quantification of growth-related variables within a stand that can inform precision management. We present a methodology to link incremental growth data obtained from tree cores with crown models derived from drone laser scanning, quantifying the relative growth condition of individual trees and their neighbours. We stem-mapped 815 trees across five stands in north-central British Columbia, Canada of which 16% were cored to quantify recent basal area growth. Point clouds from drone laser scanning and orthomosaic imagery were used to locate trees, model three-dimensional crown features, and derive competition metrics describing the relative distribution of crown sizes. Local access to water and light were simulated using topographic wetness and potential solar irradiance indices derived from high-resolution terrain and surface models. Wall-to-wall predictions of recent basal area growth were produced from the best-performing model and summarized across a grid alongside a tree-level competition index. Overall, crown volume was most strongly correlated with observed differences in 5-year basal area increment ($R^2 = 0.70$, $P < .001$). Competition and solar irradiance metrics were significant as univariate predictors ($P < .001$) but nonsignificant when included in multivariate models with crown volume. Using predictions from the best-performing model and laser-scanning-derived competition metrics, we present a newly developed growth competition index to assess variability and inform commercial thinning prescription prioritization. Growth predictions, competition metrics, and the growth competition index are summarized into maps that could be used in an operational workflow. Our methodology presents a new capacity to capture and quantify intra-stand variation in growth by combining competition metrics and measures of recent growth with high-density drone laser scanning data.

Introduction

Managing tree growth and competition

Trees face competition from their neighbours for limited resources including light, soil nutrients, water, and space. Forest inventory information can be used to derive competition indices that quantify variations in competition pressure at both tree and plot levels, which can be applied to inform upon anticipated growth rates of stem volume and basal area (Weiskittel 2011). Competition informed growth models have often been demonstrated to be more accurate than models assuming no competitive effect (Contreras et al. 2011; Gavilán-Acuña et al. 2022; Lorimer 1983). Forest managers through active management can manipulate competitive drivers of tree growth and form, for example, by applying thinning treatments that selectively remove stems to release remnant trees from competition. Thinning treatments can modify a stand's growth trajectory, wood quality, and species composition, and enhance resistance to multiple stressors such as diseases and drought (Moreau et al. 2022). They generally lead to increased diameter growth for remnant

trees and can potentially reduce the stand's rotation harvest age. Sometimes, however, thinning treatments may trigger a trade-off between maximized tree growth and decreased overall stand yield in the long term (Pretzsch 2020). Commercial thinning aims to offset treatment costs by targeting valuable dominant and co-dominant trees, while promoting growth in the remaining trees. By reducing rotation harvest age, commercial thinning can therefore play a crucial role in increasing the resilience of the timber harvest land base and providing mid-rotation fibre to mitigate potential shortages (Achim et al. 2022; Griess et al. 2019; Pinno et al. 2021b). As a result, thinning treatments are being increasingly recognized as an essential tool to improve stand structure and reduce density in the extensively managed forests of North America and Europe (D'Amato et al. 2022).

The high cost of implementing silviculture management at large scales, including thinning, has been identified as a key factor limiting its widespread adoption across Canadian provinces (Pinno et al. 2021a). In addition, localized stand responses to different intensities, timings, and patterns of thinning treatments are

Handling editor: Fabian Fassnacht

Received: November 11, 2023. Revised: May 21, 2024. Accepted: May 30, 2024

© The Author(s) 2024. Published by Oxford University Press on behalf of Institute of Chartered Foresters.

This is an Open Access article distributed under the terms of the Creative Commons Attribution License (<https://creativecommons.org/licenses/by/4.0/>), which permits unrestricted reuse, distribution, and reproduction in any medium, provided the original work is properly cited.

often poorly understood (Bose et al. 2018). Currently, operations are planned and carried out based on information collected at the stand level using ground-based plot networks. Basal area and stem density information collected from inventory plots is extrapolated to the stand level and used to determine appropriate prescriptions, typically in consideration of local knowledge, available growth models, and operator experience (Pavel et al. 2021). While generalized prescriptions for thinning treatments are relatively straightforward to implement, they may fail to sufficiently consider the intra-stand variability in tree competition and growth rates that thinning aims to manipulate, especially when applied over extensive areas, such as in North America, where it is impractical for a forester to visually assess each tree in the stand. Uniform thinning across a stand may fail to account for variation in stem density and tree size across stands and can result in inadequate release in certain areas, while sparser areas may be overharvested. This not only reduces the overall potential productivity of the stand but also inefficiently allocates limited operational resources. Beyond density regulation, thinning treatments can seek to alter species composition often through increasing the proportion of desired tree species particularly for long-term growth (Cameron 2002). To address intra-stand variability more effectively, precision forestry where thinning treatments are planned based on clusters of sub-stand sample units (e.g. pixels or grid cells) as opposed to a single stand level prescription is gaining popularity (Wilhelmsson et al. 2021). Particularly for more heterogeneous stands, this approach can better capture within-stand variations in growth pattern, density, and species composition that the thinning seeks to manipulate; however, a fundamental requirement is access to reliable, spatially explicit, fine-scale data that describe the key attributes of interest (Persson et al. 2022).

Quantifying intra-stand variability in growth with laser scanning

The implementation of precision thinning to optimize growth is limited by the availability of sub-stand level data on tree competition and basal area growth rates, which would have to be spatially quantified to prioritize operations. Fine-scale remote sensing tools, including light detection and ranging (lidar) and optical sensors mounted on drones, also known as unoccupied aerial vehicles (UAVs) or remotely piloted aerial systems, have recently become widely accessible and provide the capacity to acquire targeted tree-level structural data, which may suit this need. Drone laser scanning (lidar) or DLS has the potential to inform pre-thinning assessments, by capturing stand-level variability in tree size, competition, growth rates, stem density, and species composition more effectively than field-based stand level inventories and even area-based enhanced forest inventories (Fassnacht et al. 2016; Queinnec et al. 2023; Wilhelmsson et al. 2021). To date, fine-scale remote sensing data from drones have been successfully employed to detect and characterize individual trees across a variety of species, stem densities, and growing conditions (Chadwick et al. 2020; Goodbody et al. 2018; Leckie et al. 2017). Few studies have linked these tree locations and structural characteristics to assess distributions of competitive status across stands and model incremental growth over wide areas (Gavilán-Acuña et al. 2022). Existing examples at the tree level have most often been conducted using terrestrial laser scanning (TLS) rather than aerial lidar datasets. For example, Pretzsch et al. (2022) found a strong correlation between incremental growth patterns and measurements of crown form derived from TLS data but

did not assess tree metrics such as crown volume, local competition, and resource availability potential. Other recent efforts have continued to find strong predictive power of TLS-derived crown volume and competition metrics in explaining tree growth patterns (Ahmed et al. 2024). Tree detection and segmentation of DLS point clouds enables large-area estimation of tree locations and crown extents, enabling the computation of crown volume, competition indices derived from tree size estimates, and light and moisture resource availability variables that can be used to predict recent growth rates.

Crown volume refers to the three-dimensional size of a tree crown and is conventionally estimated using field measurements of crown width and tree height (Fernández-Sarría et al. 2013; Filipescu and Comeau 2007). Estimates of tree size, including crown volume, can serve as a proxy of key variables which determine growth rates including leaf area, light interception, and overall dominance in the canopy; however, tree size estimates are frequently only based on field measurements of tree diameter at breast height or height (Acquah and Marshall 2020; Binkley et al. 2013; Pretzsch 2021). Reliably quantifying crown volume has historically been difficult to achieve accurately with non-destructive methods and particularly at a stand scale (Zhu et al. 2021). Efforts have demonstrated the strong predictive power of crown volume derived from remote sensing techniques, including TLS, in explaining recent radial growth; however, these datasets are limited in spatial coverage (Metz et al. 2013; Ronoud et al. 2022; Seidel et al. 2015; Yrttimaa et al. 2022). DLS data combine sufficient point density to more reliably locate trees and estimate crown volume with an improved coverage enabling the collection of data across entire stands.

DLS data can also be applied to quantify key resource availability variables potentially contributing to tree growth including local solar irradiance and estimates of soil water availability (Duffy et al. 2021). High-resolution digital surface models of the forest canopy and underlying terrain, derived from DLS point clouds, allow the simulation of both the sun's rays on and into the canopy, and the topographically driven accumulation of rainfall via for example the topographic wetness index, providing an estimate of the relative availability of these resources within forest stands. These environmental variables can then serve as proxies of growth limiting factors and improve our capacity to predict growth at the tree level (Mohamedou et al. 2019).

To calibrate corresponding models using DLS-derived information, reference data for tree growth are required. Tree core samples provide measurements of growth rates that can be connected with tree-level metrics derived from remote sensing to explain spatial patterns of tree growth within stands (Babst et al. 2018). Integrating high-density (500+ points m⁻²) DLS with tree-ring data may enable the calculation of estimates of incremental growth across wider areas, providing on-demand, wall-to-wall information that is critical for managers and enables the precision implementation of thinning to optimize growth rates.

In this paper, we demonstrate a methodology that integrates high-density DLS and tree-ring data to evaluate the spatial heterogeneity of individual tree growth across managed stands; revealing tree size, competition-related and environmental drivers of recent observed tree-level growth and capturing variability across five stands. Our objectives were to (1) develop a growth model based on tree-level metrics derived from DLS data, (2) identify the best metrics able to predict recent basal area increment across managed stands, and (3) scale up the resulting model into a management ready product to guide precision thinning treatments focused on potential growth optimization. This work

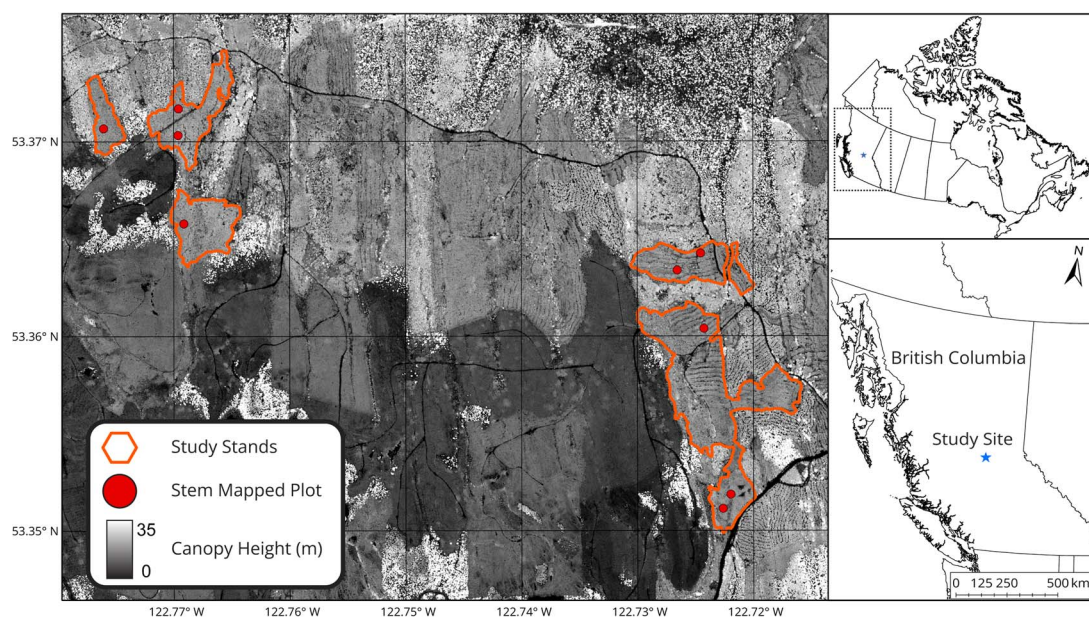


Figure 1. Location and layout of the five sampled mid-rotation stands within Tree Farm License 52, northwest of Quesnel, British Columbia, Canada. Stem-mapped plots are denoted as points overlaid on a canopy height model derived from airborne laser scanning (2021).

presents a novel workflow that combines DLS data with precisely geolocated tree core samples to produce layers intended to guide precision thinning by providing targeted description of areas within a stand where competitive release may be most needed to optimize growth.

Methods

Study area

Sampling was conducted across five even-aged stands located in Tree Farm License 52 (TFL52), a forest management tenure located northwest of Quesnel, British Columbia, Canada. The area is part of the Cariboo region of the province and is characterized by dominant coniferous tree species including Douglas-fir (*Pseudotsuga menziesii* var. *glauca* (Bessin) Franco), interior spruce (*Picea engelmannii* × *glauca* (Moench) Voss), and lodgepole pine (*Pinus contorta* Douglas var. *latifolia* (Engelm.)). The stands were selected as a representative subset of blocks within a commercial thinning cutting permit put forward by industrial partners in the area.

The five sampled stands, totalling 78 ha, were planted between 1980 and 1984 with a target density of 1600 stems per hectare and an interspersed mix of interior spruce (~50%), Douglas-fir (~40%), and lodgepole pine (~10%) (Fig. 1). Some natural regeneration has occurred along roadsides, in canopy gaps, and in areas with lower stocking of planted trees. Naturally regenerated tree species include subalpine fir (*Abies lasiocarpa* (Hooker) Nuttall), trembling aspen (*Populus tremuloides* Michx), paper birch (*Betula papyrifera* Marshall), and mountain alder (*Alnus incana* (Nutt.) Moench).

Laser scanning and imagery acquisitions

High-density laser scanning data were acquired in June 2022 with a DJI Zenmuse L1 sensor equipped with a Livox Mid70 lidar module flown on a DJI Matrice 300 RTK drone. The sensor was flown on a grid mission at a speed of 6.2 m s⁻¹ and maintained a flight altitude of 80 m above ground level, altitude was maintained through terrain following of a 1-m-resolution digital terrain model (DTM) generated from previously acquired laser scanning data. The laser scanning unit was set to a non-repetitive scanning mode

achieving a 70.4° (horizontal) by 77.2° (vertical) field of view, and collected up to three returns per pulse at a repetition frequency of 160 000 Hz; 75% overlap between flight lines resulted in an average point density of 1150 points m⁻² across the study area. The raw data from the L1 sensor was processed into standard LAS files through DJI Terra (version 3.10.7.1) with the optimize point cloud accuracy setting enabled to optimize flight lines.

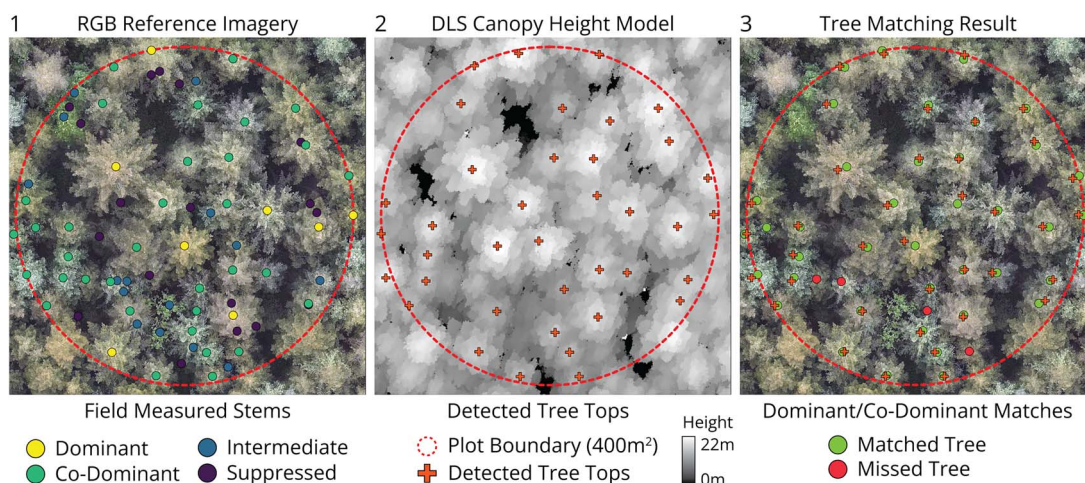
Reference optical (RGB) imagery was collected near simultaneously with the DJI P1 camera mounted on the DJI Matrice 300 RTK drone. Images were acquired at 80 m above ground level with a forward and side overlap of 85%. Photogrammetric alignment was performed on optical images producing point clouds and orthomosaic imagery with a spatial resolution of 1 cm. The settings for generation of orthomosaic imagery in Agisoft Metashape are listed in Table 1.

Field data collection

To provide a ground reference of field trees, stem mapping was conducted for 815 trees in nine plots spread across the sampled stands, simultaneously with the DLS acquisitions. Plot locations were randomly distributed and all trees >4 cm diameter at breast height (DBH) within an 11.28-m radius (400 m²) were measured and mapped. Trees within plots were numbered sequentially clockwise from the centre of the plot facing north. Species, crown class, decay class, DBH, two crown widths—one at the maximum width and one perpendicular—and disturbance indicators were recorded for all trees (Fig. 2). For a subset of 10 trees per plot, apex and base-of-live-crown heights were measured with a vertex. Tree locations were recorded with a combination of a Haglöf PosTex ultrasonic positioning tool and a Trimble Geo 7X differential GPS unit (Lämås 2010). Relative positions from the ultrasonic triangulation tool were georeferenced using a differential GPS point at the plot centre with 5–20 cm accuracy and adjusted through manual rotation of the stem map in a geographic information system with the 1-cm RGB reference imagery. Tree matching was evaluated by comparing the coordinates of tree-top maxima detected from the laser scanning data with georeferenced stem positions collected in the field; the closest two matches were assessed and the

Table 1. Options used to generate orthomosaic imagery in Agisoft Metashape.

Image alignment		Point cloud and depth map generation	
Accuracy	High	Quality	High
Generic preselection	Yes	Filtering mode	Mild
Reference preselection	Source	Max neighbours	16
Key point limit	0	Orthomosaic generation	
Tie point limit	0	Surface	DEM
Exclude stationary tie points	Yes	Blending mode	Mosaic
Guided image matching	Yes	Enable hole filling	Yes
Adaptive camera model fitting	Yes	Enable ghost filter	No

**Figure 2.** Example of reference plot used in the tree matching process. Pane 1—solid circles indicate ground reference stem map coloured by field-determined crown class and sized by diameter. Pane 2—crosses indicate automatically detected tree tops (see section 2.5), dashed line shows extent of circular plots (400 m²). RGB 1-cm reference imagery (panes 1 and 3) and DLS-derived 10-cm canopy height model (pane 2) are used as background.

shortest distance match was taken (Fig. 2). Matches beyond 2 m in distance were deemed to be false negatives. Typical accuracy metrics were computed and are reported below (Li et al. 2012). Leaning trees were recorded during plot measurement and none were found to be in excess of 2 m from the base. Matched trees were also assessed in situ during later field visits to the plots to collect tree cores and found to be highly accurate.

Across the plots, a subset of 130 stem-mapped trees were selected for tree coring in October 2022 and February 2023. At minimum 10 dominant, co-dominant, or intermediate trees were selected in each plot for coring. Each tree was cored twice using a Mora 5-mm-diameter increment borer at 1.3 m height above ground; one core was taken from the east side of the bole and the other from the south. Cores were labelled, stored in paper straws, and kept cool until they were placed in a 60°C oven and dried for 48 h. Dried cores were oriented with xylem cells facing upwards and mounted with wood glue on aspen boards. Once dry, mounted cores were sanded with 100, 120, and 600 grit sandpaper until tree-ring boundaries were clearly visible. Polished cores were scanned with an Epson Expression 12000XL, at a resolution of 2400 pixels per inch. Scanned cores were subsequently measured with Coorecorder 9.81 following the steps outlined by Maxwell and Larsson (2021). Annual ring width values were converted to basal area increment (BAI; mm² yr⁻¹), which is the change in cross-sectional area associated with each annual ring to account for relative differences in tree diameter (Bunn 2008). For each tree, cumulative BAI was calculated for the five years preceding the

sample (*sumBAI5*) to represent recent growth following canopy closure in the stand. Ring width increment (RWI) (mm yr⁻¹) and BAI values were averaged for the two cores collected from each tree. A summary of tree core variables is presented in Table 2, and a breakdown of cored trees by species and crown class is presented in Table 3.

Laser scanning data processing

Raw DLS point clouds were processed as 100-m tiles with 10-m buffers to avoid edge effects. Ground returns were classified using a cloth simulation filter (CSF), which has proven accuracy and implementation simplicity with high-density lidar data (Zhang et al. 2016). The lidR implementation of CSF was used with the following parameters: *slope_smooth*=FALSE, *class_threshold*=0.07, *cloth_resolution*=0.7, *rigidness*=2, *iterations*=500, and *time_step*=0.65. A triangular irregular network algorithm was applied to ground-classified points to produce a digital terrain model (DTM) at a 0.25-m spatial resolution. The return heights of classified lidar tiles were normalized to their height above ground level. Canopy height models (CHMs) and digital surface models (DSMs) were generated at a 0.1-m spatial resolution by applying a point-to-raster algorithm to normalized and raw lidar returns elevations, respectively. Surface models were generated at higher spatial resolution than the DTM due to the larger number of returns collected from the canopy surface. A gaussian filter with a width of five cells was applied

Table 2. Summary of cored trees included in incremental growth models ($n = 130$).

Variable	Mean	SD	Min	Max
DBH (cm)	20.7	5.1	7.6	35.3
H (m)	16.2	2.5	8.0	20.8
Crown volume (m^3)	133.9	90.6	4.8	630.6
Irradiance	0.13	0.04	0.03	0.2
TWI	4.4	0.6	3.0	6.1
BAI ($mm^2 yr^{-1}$)	972.7	675.7	3.7	4471.4
RWI ($mm yr^{-1}$)	3.2	1.6	0.12	11.7
sumBAI5 ($mm^2 5 yr^{-1}$)	10742.0	7220.5	735.7	39620.0

DBH, diameter at breast height (cm); H, tree-top height from DLS (m); crown volume, concave hull volume fit to segmented laser scanning points within each crown (m^3); irradiance, mean daily illumination value (unitless) summarized per tree crown across growing season; TWI, mean topographic wetness index (unitless) extracted for cored tree crowns; BAI, annual basal area increment from tree core samples ($mm^2 yr^{-1}$); RWI, annual ring width increment from tree core samples ($mm yr^{-1}$); sumBAI5, cumulative basal area of the 5 years preceding tree core sampling ($mm^2 5 yr^{-1}$).

Table 3. Number of cored trees ($n = 130$) field-determined species and crown class.

Tree species	Dominant	Co-dominant	Intermediate
Douglas-fir (Fd)	8	42	6
Interior spruce (Sx)	6	35	3
Lodgepole pine (Pl)	3	26	1

to smooth irregularities in the canopy height model before tree approximation.

Tree detection and segmentation were performed on the smoothed CHM. First, a local maximum filter was applied, using a 2-m circular window and a 10-m minimum height threshold, which corresponds to the minimum height of intermediate trees in our reference data (Wulder et al. 2000). Using these maxima as seeds, marker-based watershed segmentation was used to approximate crown extents (Ke and Quackenbush 2011). This top-down raster-based approach is inherently focused on identifying co-dominant and dominant trees. To reduce the tendency for segmentations to include often lower adjacent vegetation, only CHM pixels $>70\%$ of tree-top height for each segmented crown were retained (Grubinger et al. 2023). The resulting segmentations were cleaned by filling holes and retaining the largest polygon associated with each detected tree top.

Generating tree-level growth predictors

The resulting tree segmentations were used together with the DLS data products to estimate a range of tree-level metrics. These metrics were used as explanatory variables in the prediction of recent basal area growth for cored trees and in the computation of competition metrics across the study stands. Tree-level metrics included crown volume, growing season solar irradiance, topographic wetness, and a pairwise tree competition index, each of which is described in the following text.

To estimate crown volume, point clouds were first clipped to the two-dimensional extents generated from the watershed tree segmentation approach. For each clipped tree-level point cloud, crown volume was computed by generating alpha shapes, which are geometric objects that can flexibly approximate the outer shape of a set of points. Crown volume was estimated using both concave and convex alpha shapes generated using alpha values of 1 and Inf, respectively. The former produces a tighter, more detailed shape that can capture the nuances of the tree point cloud's outer boundary, while the latter expands to cover the full extent of the crown, providing a smooth boundary around each set of points (Fig. 3). The volume (m^3) of each alphashape was then

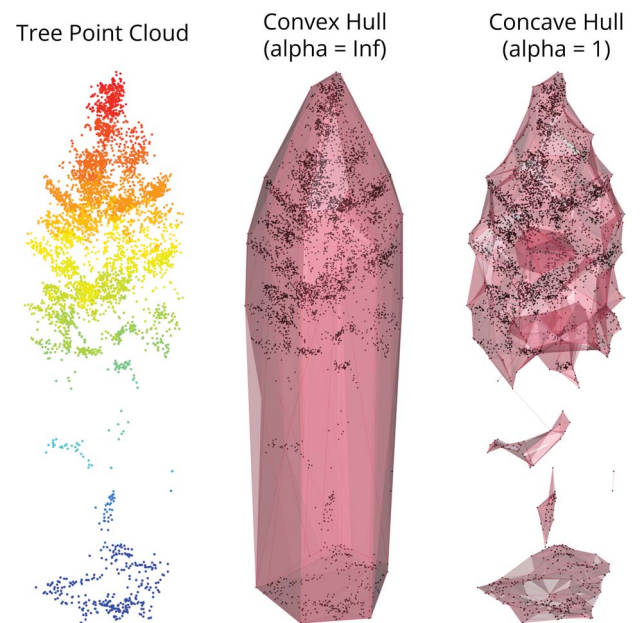


Figure 3. Example computation of three-dimensional alpha shapes from a segmented tree point cloud. Clipped point cloud is displayed on the left, convex ($\alpha = \text{Inf}$) and concave ($\alpha = 1$) alpha shapes fit to this point cloud are displayed in the centre and right.

calculated and served as an estimate of tree crown volume for further analyses.

Direct growing season irradiance was estimated for each tree crown using the laser-scanning-derived DSM and the tree segmentations (Thieurmél 2019). To estimate solar irradiance for our study stands, we simulated three time points (11 a.m., 1 p.m., and 3 p.m.) for each Monday during the growing season. A unitless index of potential direct irradiance (hereafter referred to as irradiance) was simulated across the DSM using a rayshading algorithm at each solar timepoint, considering both the zenith and azimuth angle of the sun (Morgan-Wall 2023). We then averaged the results representing mean daily irradiance received per 0.1-m

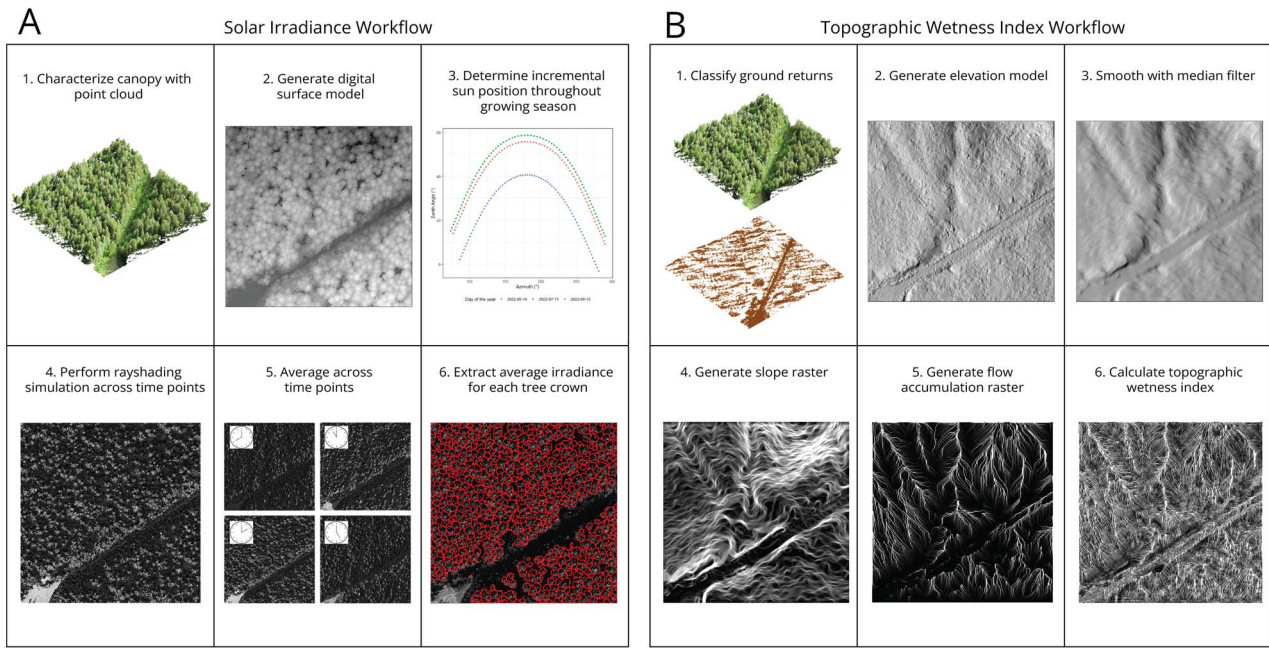


Figure 4. (A) Simulation of growing season direct irradiance; 1–2, digital surface models are generated from uppermost canopy returns of the point cloud; 3, solar position is determined for each Monday of the growing season at 11 a.m., 1 p.m., and 3 p.m.; 4, rayshading is conducted for the given solar position at each time point; 5, irradiance is then averaged across growing season timepoints ($n = 54$); 6, average growing season irradiance is extracted for each segmented tree crown. (B) Characterization of fine-scale topographic wetness across study area; 1, ground classification is conducted on lidar returns; 2, digital terrain model is generated from ground returns; 3, digital terrain model is smoothed with a median filter; 4, slope raster is calculated as the difference between cells; 5, flow accumulation is estimated; 6, topographic wetness index is calculated from constituents and the mean value is extracted for tree crowns.

pixel throughout the growing season (Fig. 4A). The mean value of this raster was extracted for each tree crown (*irr_mean*) and used in further modelling efforts. This approach accounted for solar position, topography, and estimated total potential direct canopy irradiance. In real-world conditions, actual values will be lower due to cloud cover (Jennewein et al. 2021).

To estimate potential surface water flow, the topographic wetness index (TWI), also known as the compound topographic index (Fig. 4B), was calculated. Slope and flow accumulation were estimated from the 0.25-m DTM and used as inputs to determine TWI for each cell (Sørensen et al. 2006). The mean TWI values were then extracted for each tree crown (*twi_mean*) and used in further modelling efforts.

Finally, established techniques for quantifying competition as an index were applied to the detected trees using a pairwise distance-dependent equation which weights the influence of neighbouring trees based on their size (within the sphere of influence) relative to their distance from the target tree (Heygi 1974). This approach relies on field measurements of tree size such as top height and diameter. However, it is now increasingly common to use three-dimensional tree size metrics that can be more readily derived from remote sensing such as tree crown volume/area (Ronoud et al. 2022). In our case, the distance-dependent competition index was applied to crown volume (*convex_hull*) values derived from the DLS data to describe the local competition experienced by each detected tree (Fig. 5) (Heygi 1974). A 6-m radius sphere of influence around each target tree was used which approximates 3.5 times the average crown radius (1.7 m) (Contreras et al. 2011; García 2014).

$$CI = \sum_{i=1}^n \frac{X_i}{(X \times dist_i)} \quad (1)$$

Here, *CI* is the competition index value for a target tree, *X* is the crown volume for the target tree, X_i is the crown volume for the competitor tree *i*, $dist_i$ is the Euclidean distance from the target tree to the competitor tree *i*, and *n* is the number of competitor trees within the sphere of influence.

Modelling recent basal area growth

Tree-level growth predictor variables were calculated for each individual tree segmented across the study area (Table 4). Tree segmentations attributed with predictor values that were positively matched to cored trees ($n = 130$) were isolated and used for model development. To address the hierarchical nature of our sampling design where cored trees are grouped together in plots, we used linear mixed-effects models to incorporate plot identity as a random effect. We included plot as a random intercept to account for variability in growth patterns between plots and correlated error structures. The significance of the random plot effect was based on the likelihood ratio test ($P < .05$) between nested models (Pinheiro and Bates 2000). We used the cumulative basal area increment of the last 5 years (*sumBAI5*; $\text{mm}^2 \text{ 5 yr}^{-1}$) as the response variable to capture the range of recent growth patterns in the cored trees ($n = 130$). Natural log transformations were conducted on the response and explanatory variables to satisfy the assumptions of linearity and homogeneity of residuals. The general form of a linear mixed-effects model is as follows (Eq. 2):

$$\log(\text{sumBAI5}_{ij}) = (\beta_0 + b_{0j}) + \beta_1 V_1 + \dots + \beta_n V_n + \epsilon_{ij} \quad (2)$$

where sumBAI5_{ij} represents the 5-year periodic total basal area increment for the *i*th tree measured at the *j*th plot, β_0 is the intercept, and β_1, \dots, β_n are the parameters estimated for the

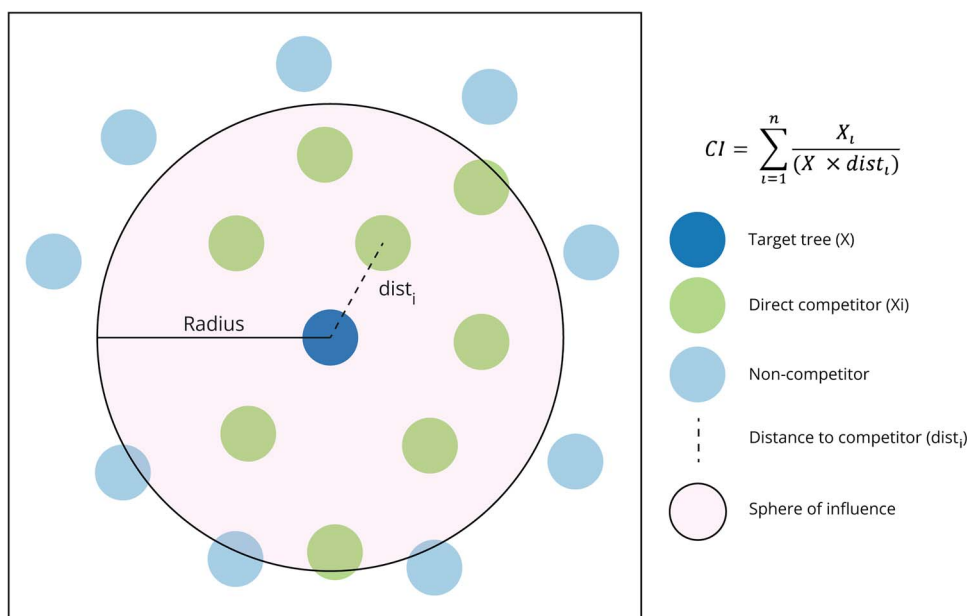


Figure 5. Calculation of pairwise competition index within the sphere of influence (6-m radius) surrounding each target tree. X = target tree size, X_i = competitor tree size, $dist_i$ = Euclidean distance from target tree to competitor, n = number of competitor trees within sphere of influence.

corresponding covariables V_1, \dots, V_n , b_{0j} is the plot level random effect, and ϵ_{ij} is the error term that is assumed to be independent and normally distributed with a mean of zero and constant variance, $b_{0j} \sim N(0, \sigma_0^2)$ and $\epsilon_i \sim N(0, \sigma_{res}^2)$. A suite of univariate and multivariate models was generated to test different combination of variables listed in Table 4. Interactions between predictor variables were not incorporated in the model selection process due to the associated difficulty interpreting interactions between continuous variables. The corrected Akaike information criterion (AICc) was used to select the best candidate model as the ratio between the number of data points and the number of model parameters ratio fell <40 when more than one predictor variable was included (Burnham et al. 2010). The model with the lowest AICc was used as the full model for subsequent prediction of wall-to-wall recent basal area increment growth, $\log(\text{sumBAI5})$. Logarithmic predictions applied outside of plot boundaries were back transformed to their original scale considering only estimates from the fixed-effects model.

To evaluate the reliability of the best candidate model, we conducted a leave-one-stand-out cross-validation. In each iteration, a model was trained on data from four stands and evaluated on the trees in the remaining stand. To evaluate the cross-validation, adjusted R^2 , bias, model efficiency, and root mean squared error (RMSE) were calculated for each iteration and averaged (Riofrío et al. 2019).

Overlay prioritization analyses

With the aim of operationalizing the modelling results, we applied predictions of 5-year BAI and computed the DLS-derived competition index for all individual trees segmented beyond plot boundaries. From this information, we formulated a new growth competition index (GCI) intended to capture two key pieces of information across the stand and their variability, the first being the range of predicted BAI growth values, and the second, a representation of the spatial distribution of tree sizes relative to their neighbours across the stand. Once applied across the stand, we analysed the spatial patterns of predicted growth,

laser-scanning-derived competition, and the GCI, and summarized these results across a grid to facilitate operational use and interpretation.

The goal of the GCI is to describe trees in terms of their relative growth and laser-scanning-derived competition and identify trees with high competition index and low predicted growth as high priority for thinning. Due to differences in the distributions and magnitudes of sumBAI5 predictions and cindex, both were normalized across all trees for each stand based on the minimum and maximum values. Next, for each tree we calculated GCI using the following formula:

$$GCI = \frac{(1 - \text{sumBAI5}_{norm}) + \text{cindex}_{norm}}{2} \quad (3)$$

GCI describes the distribution of predicted growth and the derived competition metric across the stand and can be used as a relative thinning priority indicator to map variability in these metrics. Values ranged from zero to one, with values closer to one indicating relatively high competition and low growth, values closer to zero representing trees where growth was relatively high and competition low, and intermediate values suggesting similarity between the two metrics.

As a demonstration, summary grids were calculated that can be used to guide precision commercial thinning operations towards clusters of high-priority cells (Wilhelmsson et al. 2021). For this, predicted 5-year BAI (sumBAI5) and the pairwise competition index (cindex) were summed for all trees falling within 2500-m² (0.25 ha) hexagonal cells covering each stand. Hexagons were chosen over a square grid to reduce edge effects associated with summarization, improve the clarity of visualizations, and better integrate with existing polygonal forest inventory systems (Birch et al. 2007).

The cumulative and mean GCI was extracted for all trees falling within each hexagonal summary cell to describe the distribution of these values across the stands. Finally, summary grids were clipped to the established boundaries of the operational stands to improve interpretability and reduce the influence of forest area adjacent to the study stands.

Table 4. Variables included in basal area increment models.

Explanatory variables	Data source	Ecological justification	Range (mean/min/max/SD)
Crown volume (vol_convex and vol_concave)	Alphashape model based on 3D tree segmentation	Incorporates three-dimensional crown structure of neighbouring and target trees	vol_convex: (101/5/349/61) vol_concave: (29/1/120/19) Units = m ³
Solar irradiance (irr_mean)	Digital surface model (DSM) together with localized raytracing model across the growing season	Accounts for shading impacts of canopy and surrounding trees on the amount of sunlight intercepted by the target tree	(0.15/0.03/0.25/0.05) Unitless
Tree height (Zmax)	DLS-derived local maxima tree-top height	Tree height is a simple proxy of tree dominance, its relation to neighbouring tree heights indicates the degree to which the target tree has foliage above its neighbours	(16.6/10.1/21.2/2.4) Units = m
Topographic wetness index (twi_mean)	DLS-derived digital terrain model (DTM)	Accounts for microtopographic differences in potential soil moisture available for each tree	(4.3/2.9/6.7/0.7) Unitless
Pairwise competition (cindex)	Neighbourhood analyses of crown volume (vol_convex)	Distance-dependent tree size indices have been long used as covariables in tree growth models as they describe a tree's relative dominance and resource availability	(5.0/0.5/65.6/6.8) Unitless
Tree diameter (DBH)	Calliper field measurements	Diameter is the status quo for assessing the potential growth and competitive status of trees in a forested stand and is easily obtained for plot measurements	(20.5/7.6/35.3/5.2) Units = cm
Response variables			
Recent basal area increment (sumBAI5)	Tree-ring width measurements from core samples	BAI is driven in large part by a tree's ability to maintain competitive status and obtain sufficient sunlight for sustained growth; we took the cumulative growth over the last 5 years to describe the recent growth pattern of each sample tree. Generally, tree growth models estimate basal area increments in 5-year bins	(4726.3/278.7/17330.3/2987.6) Units = mm ² 5 yr ⁻¹

Range of values for cored trees presented in final column including mean, minimum, maximum, and standard deviation.

Software used

R Packages used for this study included lidR for all lidar preprocessing including tile division, buffering, ground return classification, and the generation of DTMs, CHMs, and DSMs (Roussel et al. 2020). lidR was also used to detect local maxima and conduct marker-based watershed tree segmentation. Tree core measurements were processed into basal area increment using dplR (Bunn 2008). The estimation of crown volume used the alphashape3d package to compute three-dimensional hulls associated with each segmented point cloud (Lafarge and Pateiro-Lopez 2014). Surface water flow and its accumulation were estimated using the Whitebox tools package in R to compute a TWI raster based on the DLS DTM (Lindsay 2014; Sørensen et al. 2006). The simulation of solar irradiance was conducted with the rayshader package (Morgan-Wall 2023). The siplab and spatstat packages enabled the calculation of distance-dependent competition indices (Baddeley and Turner 2005; García, 2014). Orthomosaics used for tree matching were generated from drone images in Agisoft Metashape Professional Version 2.0 (Agisoft LLC, St. Petersburg, Russia). Finally, linear mixed-effect modelling was conducted in R with the lme4 package (Bates et al. 2015).

Results

Tree matching

The results of tree detection were validated with the georeferenced ground measured stem maps. Accuracies were high for dominant and co-dominant stem achieving recalls and F-scores

of 0.95/0.98 and 0.78/0.88, respectively. Intermediate and suppressed stems had much lower recall and F-scores of 0.12/0.22 and 0.09/0.17, respectively. A summary of tree matching accuracy by field-determined crown class is reported in Table 5. All 130 trees from which cores sampled were successfully matched with tree tops detected in the canopy height model.

Basal area increment model

Results from the model selection process to predict recent basal area growth (sumBAI5) of the individual trees sampled in our stands indicated a strong effect of crown volume (vol_convex) in explaining variation when the random effect of plot was included (marginal $R^2 = 0.70$). Other variables including solar irradiance (irr_mean), pairwise competition (cindex), tree height (Zmax), and field-measured diameter (DBH) were also found to be significant predictors when included on their own ($P < .05$) but nonsignificant when included in multivariate models alongside crown volume (vol_convex) (Table 6). To investigate other combinations, all possible models were examined; however, the simplest model which included only log-transformed crown volume (vol_convex) and the random effect of plot consistently had the highest performance and predictive power (AIC = 150.0, marginal $R^2 = 0.70$, conditional $R^2 = 0.62$) (Eq. 4). The performance of a subset of the tested models including all univariate and selected multivariate models including crown volume (log_vol_convex) and the top univariate predictors (log_vol_concave, log_irr_mean, cindex, Zmax) are reported in Table 6. The leave-one-stand-out cross-validation of the fixed-effects model resulted in an average adjusted R^2 of 0.59, back-transformed RMSE of 209mm² 5 yr⁻¹ (42.3% of mean),

Table 5. Results of tree matching accuracy assessment between ground reference stems and lidar detected tree-top maxima.

	Dominant	Co-dominant	Intermediate	Suppressed
N Reference	42	403	114	65
N Detected	40	314	14	6
True positives	40	314	14	6
False negatives	2	89	100	59
Recall	0.95	0.78	0.12	0.09
F-Score	0.98	0.88	0.22	0.17
Max/min distance (m)	2.68/0.008	3.33/0.002	3.37/0.01	2.17/0.02
Mean/SD distance (m)	0.97/0.79	1.03/0.88	1.38/0.89	1.26/0.77

Standard accuracy metrics were generated as following the approach demonstrated in Li et al. (2012). Accuracy metrics are reported by field-determined crown class.

Table 6. Summary of 5-year BAI linear mixed-effects modelling efforts.

Model number	Univariate models					Multivariate models					Diameter
	1	2	3	4	5	6	7	8	9	10	
(Intercept)	4.76***	6.24***	10.27***	8.60***	8.83***	5.41***	4.94***	5.43***	5.29***	4.64***	6.17***
log_vol_convex	0.75*** (0.051)						0.64*** (0.16)	0.70*** (0.062)	0.65*** (0.079)	0.72*** (0.069)	
log_vol_concave		0.62*** (0.047)					0.10 (0.14)				
log_irr_mean			0.94*** (0.14)					0.19 (0.11)			
cindex				-0.06*** (0.0055)					-0.01 (0.0070)		
twi_mean					-0.12 (0.096)						
Zmax						0.17*** (0.023)				0.02 (0.022)	
Diameter											0.10*** (0.0075)
σ_0^2	0.039	0.031	0.046	0.034	0.038	0.038	0.073	0.038	0.036	0.044	0.0075
σ_{res}^2	0.15	0.17	0.30	0.23	0.42	0.42	0.28	0.15	0.15	0.15	0.18
R ² Marginal	0.62	0.57	0.25	0.42	0.012	0.33	0.62	0.62	0.62	0.62	0.60
R ² Conditional	0.70	0.64	0.35	0.49	0.10	0.47	0.70	0.70	0.70	0.70	0.62
AICc	150.3	165.3	234.2	207.3	274.3	232.4	154.1	152.3	157.9	157.8	165.0
Δ AICc	0	15.0	83.9	57.0	124.9	82.1	4.8	2.9	7.6	7.5	14.7
RMSE	0.38	0.40	0.53	0.47	0.63	0.52	0.38	0.37	0.37	0.38	0.41

Predictor variables listed on left with associated coefficients, significance, and standard errors in brackets beneath. Models with single variables are listed in models 1–6, and multivariate models in 7–10. Model 11 is based on field-measured diameter alone. *P < .05, **P < .01, ***P < .001.

bias of -0.030, and model efficiency of 0.39.

$$\text{sumBAI5} = \exp(4.75962 + 0.75351 * \log(\text{vol_convex})) \quad (4)$$

Thinning prioritization analyses

Summarizing growth and competition estimates across all five stands resulted in gridded maps of cumulative basal area growth, competition, and relative thinning priority (GCI) (Fig. 6, Fig. 7). Across all five stands, cumulative growth values within grid cells (2500 m²) ranged from 248 706 to 2 277 036 with a mean of 1 268 934 (312 429 SD) mm² 5 yr⁻¹. Cumulative competition values ranged from 181 to 2851 with a mean of 834 (323 SD). Average values of GCI within grid cells ranged from 0.14 to 0.71 with a mean of 0.47 (0.06 SD) (Table 7). Cumulative BAI rates were converted from square millimetre to square metre to improve the readability of the following figures and table.

Discussion

This study investigated the suitability of tree-level metrics derived from drone laser scanning to explain variability in recent basal

area growth and indirectly map competition across trees in managed stands. The selected basal area growth model was applied across the five study stands alongside laser-scanning-derived competition. Our results suggest that recent basal area growth (sumBAI5) was most strongly linked to crown volume (convex_hull) which enabled the prediction of recent growth, the derivation of a competition metric, and the synthesis of a thinning priority index across a regular summary grid. The intended users of this type of drone-derived product would be silvicultural managers implementing commercial thinning operations across large areas where individual tree-level selection is not feasible but where broader level prioritization using 0.25-ha cells could be guided across treatment units (Wilhelmsson et al. 2021). Through this approach, intra-stand variability in both growth and competition metrics can be captured and used to optimize growth gains from thinning removals. The focus of this study was to present a workflow focused on optimizing growth in the form of basal area increment with commercial thinning, with the goal of reducing stand rotation age (Griess et al. 2019). Thinning treatments can, however, also be implemented to support other management objectives including manipulating wood quality,

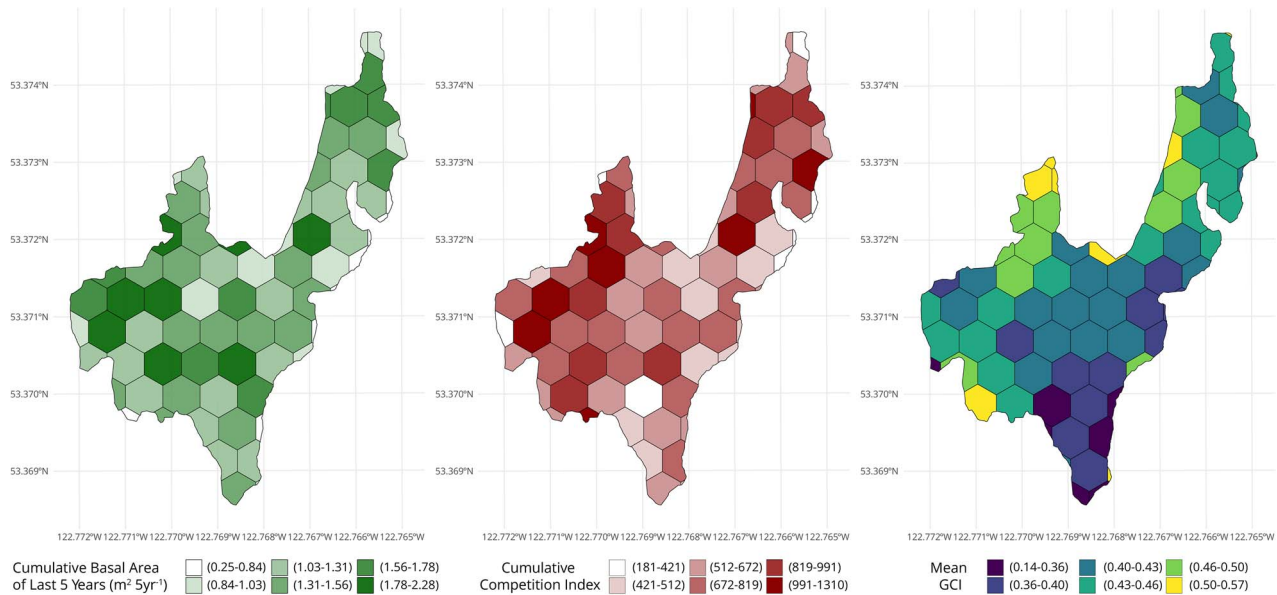


Figure 6. Example summary maps for study stand. CT1, cumulative basal area growth, competition, as well as mean GCI values are displayed for each grid cell (0.25 ha). Gradients represent percentile breaks for values from 0 to 10, 10-25, 25-50, 50-75, 75-90, and 90-100% of values.

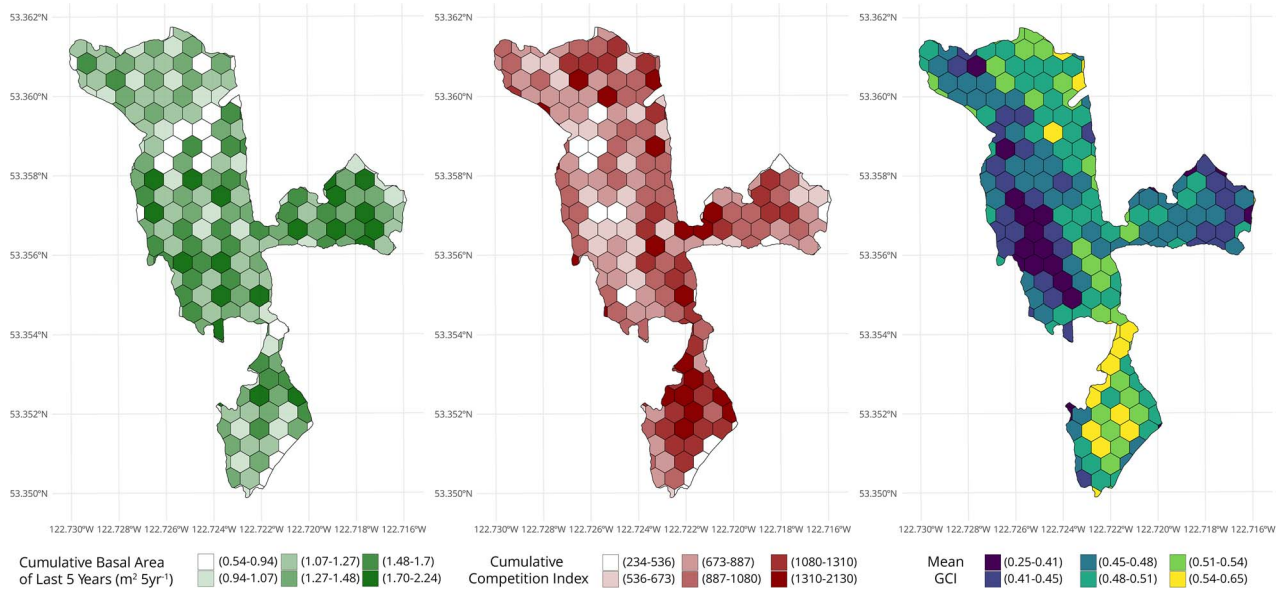


Figure 7. Example summary maps for study stand. CT5, cumulative basal area growth, competition, as well as mean GCI values are displayed for each grid cell (0.25 ha). Gradients represent percentile breaks for values from 0 to 10, 10-25, 25-50, 50-75, 75-90, and 90-100% of values.

Table 7. Summary statistics for grid cells contained in the five study stands ($n = 447$).

Metric	Mean	SD	Minimum	Maximum
Cumulative BAI ($m^2 \text{ 5 yr}^{-1}$)	1.27	0.31	0.25	2.28
Cumulative competition	834	323	181	2851
Cumulative GCI	89.1	54.0	0.14	247.9
Mean GCI	0.47	0.06	0.14	0.71

Mean, standard deviation (SD), minimum and maximum values are reported for all grid cells (0.25 ha) across the five study stands.

and increasing resistance to disturbances including forest pests, drought, and wildfire (Moreau et al. 2022). These objectives would require their own specialized prioritization schemes which are not covered by this work but could be informed by it. In the following sections, the results of modelling efforts, the effectiveness

and influence of tree detection, and the utility of the drone-based forest inventories to inform precision forest management are discussed, along with considerations for future research and operational applications of the approach demonstrated herein.

Predicting recent growth with tree-level laser scanning metrics

Crown volume (convex hull) had the strongest ability to explain variation in observed recent basal area increment growth of the cored trees in our study. High-density drone laser scanning data and automated tree segmentation processes enabled the estimation of crown volume for all observable trees across large areas facilitating the prediction of recent BAI. Moreover, crown measurements derived from drone or terrestrial laser scanning data are able to accurately capture the influence of neighbouring competitors on individual tree crowns in spatially diverse canopies (Barbeito et al. 2017; Metz et al. 2013). The model (11) based on solely field-derived DBH showed a reduced ability (marginal $R^2=0.62$) to explain variability in recent basal area growth than the model using crown volume (vol_convex) (marginal $R^2=0.70$). This finding suggests that in these stands, DLS-derived crown volume not only provides the benefit of wall-to-wall coverage compared to DBH, but also served to better predict growth of the cored trees. We recognize, however, that variability in growth due to unmeasured factors, including tree species, genetics, site productivity, past management actions, and undocumented disturbance agents, likely limit the strength of this relationship. Despite these sources of variability, leave-one-stand-out cross-validation of the selected model indicated fair performance and allowed prediction across stands and the calculation of spatially explicit growth rates estimates and competition metrics.

The growth of other mixed coniferous stands in central British Columbia has been previously tied primarily to aboveground competition for light resources (Acquah and Marshall 2020). The relationship observed between BAI, crown volume, pairwise competition, and solar irradiance indicates the strength of light-dependent drivers in determining growth rates (Table 6). In our results, when included in predictive models with crown volume, solar irradiance and competition became statistically insignificant, likely reflecting redundancy in the information captured by crown volume (tree size) and these related metrics as larger crowns dominate their neighbours, and capture light more effectively (Binkley et al. 2013; Gspaltl et al. 2013).

Topographic wetness index was found to have no significant relationship with recent BAI, even as a sole predictor. It is possible that a lack in variation of surface topography across plots in this study obscured the influence of topography, or that surface moisture is not a limiting factor to growth in the examined stands.

Retrospective analysis of tree growth pattern using increment borers is a classic data source to develop local forest growth models (Riofrío et al. 2019). Obtaining highly accurate measurements from tree cores requires labour-intensive processing in the field and laboratory to collect, prepare, scan, and quantify each ring width boundary (Maxwell and Larsson 2021). Integrating these measurements into fine-scale inventories based on remote sensing comes with its own set of challenges; primarily, the precise geolocation and matching of cored trees. Ensuring a positive match between cored trees and detected trees was instrumental to building a reliable model based on tree-level metrics. In our case, we found that the use of highly accurate differential GPS, ultrasonic triangulation of stem-mapped trees, and adjustment of georeferenced stem maps using coincidentally acquired high-resolution imagery were critical steps to ensure strong model correspondence. In this study, we were successfully able to geolocate all trees where tree core samples were taken. However, users of this method interested in sample subordinate crown classes should carefully adapt their tree detection strategies accordingly.

Influence of the tree detection process

The efficacy of individual tree detection and segmentation approaches from remotely sensed data including drone-based sensors has been thoroughly explored in recent years and continues to be refined (Chehreh et al. 2023). Overall, many limitations and site-specific patterns have been established in applying the process across the world's forests. Specifically, the tendency for individual tree segmentation—particularly raster-based approaches—to miss occluded trees is often cited as problematic (Hamraz et al. 2017). In this study, dominant and co-dominant trees were targeted as they are of principal economic interest in commercial thinning from above. Tree detection accuracy for dominant and co-dominant trees across our stands was high (F -score = 0.98/0.88); however, the raster-based segmentation approach unsurprisingly failed to capture the majority of intermediate and suppressed trees (F -score = 0.22/0.17). In the dense study stands, the majority of suppressed trees were found to have already experienced competition-induced mortality, and likely do not significantly contribute to basal area growth or affect the growth of dominant and co-dominant trees through competition.

We chose well-demonstrated, computationally simple methods for individual tree detection in even-aged coniferous stands, a forest type that has been proven compatible with the approach overall (Jakubowski et al. 2013). The over- and under-segmentation of overstory trees with this approach cannot be avoided and therefore the accuracy metrics (Table 5) presented reflect the impact of potential bias associated with these errors. Higher density laser scanning datasets particularly in terms of their understory coverage, combined with modified tree detection approaches capable of segmenting suppressed and intermediate trees, could enable a similar approach to be implemented to improve the reliability of the approach and support prioritization of thinning from below (Hamraz et al. 2017).

Manipulating species composition is often an objective of thinning efforts as the growth of high-value species can be prioritized by targeting removal efforts towards lower value species. Tree species and inter-species competitive interactions also affect incremental growth patterns within a stand (Pretzsch and Schütze 2009; Zhao et al. 2006), and might also modify canopy packing and crown allometry through species interactions. However, species information was not included at this stage in our wall-to-wall predictions and we recognize including species labels of segmented trees as a predictor of basal area increment may enable a more robust approach while simultaneously providing a compositional layer for further prioritization of thinning efforts. Future work will examine the possibility of automatically estimating species from these high-density point clouds and adding this information into the workflow.

Wall-to-wall summaries

The application of the predictive model to tree crowns segmented outside of plot boundaries enabled the assessment of intra-stand variability in recent BAI, derived competition metrics, and the growth competition index. Operationally, the specifics of the summarization process will depend on the forest management scale and framework that users choose to implement. However, summing or averaging estimates across equally sized cells provides a suitable baseline for further prioritization efforts and clustering (e.g. Wilhelmsson et al. 2021). The summary layers we produced display a wide range of values for the growth predictions, competition metrics, and priority index which visually appear to be clustered (Fig. 6, Fig. 7). Depending on machine and operator

availability, as well as other objectives, managers can view these maps in a GIS and determine a suitable threshold GCI value to determine a cell's inclusion and intensity in the thinning operation. By allocating less time to lower priority areas of a stand (e.g. $GCI < 0.3$), operator hours can be shifted to more intensely thin other areas within and across other nearby stands. The utility and calibration of this GCI threshold could be confirmed through stand visits with foresters who are experienced in visually assess thinning priority from the ground.

Our study focused on the development of a pre-thinning prioritization inventory; however, future work can also investigate the utility of integrating wall-to-wall BAI estimates to evaluate the actual efficacy of thinning treatments, the outcomes of which have been shown to depend on the approach, intensity, and timing (Bose et al. 2018). Following thinning efforts in the stands analysed here, the expected reaction of remnant trees would be an increase in overall crown volume in response to increased lateral growing space and light availability. Conducting similar analyses once crowns and tree growth patterns have had sufficient time to react to the competitive release associated with the thinning can enable managers to assess variability and effectiveness realized as increases in basal area growth (Bose et al. 2018). As a result, subsequent drone-based surveys 5 or 10 years following treatments can quantify crown volume expansion, competition status changes, and link these metrics with tree growth enabling spatially explicit quantification of the impact of thinning on basal area or volume increment at a sub-stand level. Moreover, repeated quantification of tree increment and growth allow comparison of the short- and long-term effects of stand density regulation on the growth and yield of forest stands (Pretzsch 2020; Zeide 2001). Managers can compare the results of growth and competition trends derived from remote sensing to investigate the spatial distribution of growth rate changes across stands and how these relate to thinning prescriptions. Generating bi-temporal laser scanning assessments across a range of stand conditions could enable the development of generalizable remote sensing-driven predictions of growth increases resulting from thinning, allowing the evaluation of net effects across differing competition, structural, and compositional configurations (Tompalski et al. 2021).

Collection of drone-based forest inventories

In this study, the remote sensing and field datasets were collected well in advance of any operations to allow for sufficient time to process, integrate, and interpret the datasets, particularly the tree core samples which required time-consuming manual measurement. As computation power increases and open-source tools become more easily accessible for managers, the time gap between data acquisition and the generation of a prioritization layer will decrease (Roussel et al. 2020). Reduced technological constraints in information processing, and demonstrations of measurement and prioritization frameworks to map distributions of intra-stand variability in basal area growth will serve to streamline the planning of spatially explicit precision thinning operations.

To prioritize the application of commercial thinning in managed stands, the timing of drone laser scanning acquisitions should also be determined strategically with stand successional stage. Users of this approach should time data acquisitions following canopy closure, during the period in which the effect of density on growth is maximal and competition-induced effects among trees are actively reducing overall productivity (Pretzsch 2020; Thurm and Pretzsch 2021). Ideally, these data should be

collected before significant stand mortality driven by resource competition has occurred, which could reduce the potential yield of the stand (Bose et al. 2018).

The exact timing of both thinning treatments and pre-thinning data collection will depend on local forest structure and composition and should be informed by expert judgement, and data-driven understanding of localized response to the timing of thinning interventions. Optimal timing can be determined for example by assessing changes in relative volume growth demonstrated in stands before and after thinning; however, this relationship is dependent on site, species, density, and intensity of the thinning (Bose et al. 2018). As fine-scale remote sensing tools are more broadly integrated into both the planning and evaluation of thinning treatments, the optimal timing and intensity of treatments may become clearer.

Integrating fine-scale forest inventory data into management

Fine-scale estimates of relative tree growth are only useful in a management context to the extent which they can be actively integrated in existing operations. Modern single tree harvesting systems are now capable of using raster and polygonal forest inventory layers on on-board computers which are displayed to the operator in real time during the application of thinning treatments (Keefe et al. 2022). In Canada as well as other jurisdictions internationally, a shift is underway as companies and institutions move from traditional stand-level polygonal inventories towards pixel-based enhanced forest inventories typically derived from airborne laser scanning (Fassnacht et al. 2023). Simplifying these detailed forest inventory estimates while ensuring adequate coverage that captures intra-stand spatial variability is key to successfully integrating these data into effective management decisions. In this study, we achieved this through summarization across a 0.25-ha grid, leaving the remainder of planning to interpretation by the forest manager. Future research can focus on the direct integration of remotely sensed forest attributes into automated planning systems that accommodate operational constraints, management objectives, and established local practices for thinning intensity and pattern (Wing et al. 2019).

Integrating fine-scale inventory data into precision planning can improve the efficiency and economic viability of forest management with limited operational resources (Gülci et al. 2015). Mapping the distribution of thinning efforts may also improve the prediction of gains from the induced growth effect as well as the quantification of timber yields from the thinning treatments themselves. Persson et al. (2022) compared stand-level to pixel-level (precision) thinning across conifer-dominated forests in Sweden and demonstrated that precision methods resulted in more consistent distributions of residual basal area indicating a successful capture of within-stand variation with these techniques. While these authors noted only marginal economic benefit to operations with their precision methods, improvements in quantifying and mapping within-stand variation such as those presented herein may increase the value generated by these approaches (Persson et al. 2022).

This study summarized the results of the individual tree approach on a regular grid (a map) to guide large-area thinning prioritization in a western Canadian management context. A similar approach could be implemented under different circumstances where management occurs over smaller areas and/or at the tree level to precisely target high-priority trees (Keefe et al. 2022). However, this requires careful consideration as it would require highly accurate and reliable connections to

Global Navigation Satellite Systems (GNSS) for both the harvester head and operator. Under canopy cover and particularly with lower cost GNSS receivers, the positioning error of these systems can exceed 7.0 m making this potentially unreliable particularly in high-density stands which are often the target of thinning (Hauglin et al. 2017).

Conclusion

In this study, we developed and demonstrated a new methodology to link intra-stand variability in tree growth to competition metrics and individual tree metrics derived from remote sensing within five managed stands. Among several predictors, convex-hull crown volume derived from laser scanning was the best predictor of recent growth and was used to model recent basal area increment and derive competition metrics across these large areas. We synthesized our growth predictions and competition metrics into a new GCI which was then summarized across a regular grid and provided as maps to inform forest managers during the prioritization of thinning operations to optimize basal area growth. This work presents a novel application of drone laser scanning in forest management and outlines a straightforward approach to integrate tree-ring growth data with fine-scale remote sensing to answer operational and research questions. As drone systems and the associated processing workflows become increasingly capable, available, and affordable, they will continue to provide critical, timely information which can increase the efficiency and efficacy of silvicultural management including commercial thinning.

Acknowledgements

Our thanks to the anonymous contributors and editors involved in the peer review process of this manuscript—thank you very much for your valuable time and careful feedback. Many thanks as well to all the field assistants involved in the data collection process including Sergio Alonso-Sanchez, Tommaso Trotto, Ramon Melser, Dr Andrew Chadwick, Dr Rik Nuijten, Dr Omar Mogni, Pablo Valle Medrano, Solo Reonato Rizzi, Dr Lukas Winiwarter, and Dr Christopher Mulverhill. Topical and logistical support was provided by industry partners at West Fraser, Quesnel. Special thanks to help with the tree core processing provided by Dr David Montwé, Fleur Damen, and Mustafa Sirajul.

Author contribution

Liam Irwin (Conceptualization, Data curation, Formal analysis, Investigation, Methodology, Resources, Software, Validation, Visualization, Writing – original draft, Writing – review & editing), Nicholas Coops (Conceptualization, Funding acquisition, Project administration, Resources, Supervision, Writing – original draft, Writing – review & editing), José Riofrío (Conceptualization, Formal analysis, Methodology, Supervision, Validation, Writing – review & editing), Samuel Grubinger (Formal analysis, Methodology, Software, Writing – review & editing), Ignacio Barbeito (Conceptualization, Investigation, Methodology, Supervision, Writing – review & editing), Alexis Achim (Formal analysis, Funding acquisition, Investigation, Methodology, Project administration, Resources, Supervision, Writing – review & editing), Dominik Roeser (Conceptualization, Resources, Supervision).

Conflict of interest: None declared.

Funding

This research was conducted as part of the Silva21 Alliance Grant Project (NSERC ALLRP 556265-20) funded by the Natural Sciences and Engineering Research Council of Canada led by Dr Alexis Achim.

Data availability

The data that support the findings of this study are available from the corresponding author on reasonable request. A demonstration of the competition metric and crown volume generation including code and a subset of the study dataset can be found on GitHub at the following link: <https://liamirwin.github.io/CompTreeR/>.

References

- Achim A, Moreau G, Coops NC. et al. The changing culture of silviculture. *Forestry* 2022;**95**:143–52. <https://doi.org/10.1093/forestry/cpab047>.
- Acquah SB, Marshall PL. Assessing differences in competitive effects among tree species in Central British Columbia, Canada. *Forests* 2020;**11**:167. <https://doi.org/10.3390/f11020167>.
- Ahmed S, Hilmers T, Uhl E. et al. Neighborhood competition modulates the link between crown structure and tree ring variability in monospecific and mixed forest stands. *For Ecol Manage* 2024;**560**:121839. <https://doi.org/10.1016/j.foreco.2024.121839>.
- Babst F, Bodesheim P, Charney N. et al. When tree rings go global: challenges and opportunities for retro- and prospective insight. *Quat Sci Rev* 2018;**197**:1–20. <https://doi.org/10.1016/j.quascirev.2018.07.009>.
- Baddeley A, Turner R. Spatstat: an R package for analyzing spatial point patterns. *J Stat Softw* 2005;**12**:1–42. <https://doi.org/10.18637/jss.v012.i06>.
- Barbeito I, Dassot M, Bayer D. et al. Terrestrial laser scanning reveals differences in crown structure of *Fagus sylvatica* in mixed vs. pure European forests. *For Ecol Manage* 2017;**405**:381–90. <https://doi.org/10.1016/j.foreco.2017.09.043>.
- Bates D, Mächler M, Bolker B. et al. Fitting linear mixed-effects models using lme4. *J Stat Softw* 2015;**67**:1–48. <https://doi.org/10.18637/jss.v067.i01>.
- Binkley D, Campoe OC, Gspaltl M. et al. Light absorption and use efficiency in forests: why patterns differ for trees and stands. *For Ecol Manage* 2013;**288**:5–13. <https://doi.org/10.1016/j.foreco.2011.11.002>.
- Birch CPD, Oom SP, Beecham JA. Rectangular and hexagonal grids used for observation, experiment and simulation in ecology. *Ecol Model* 2007;**206**:347–59. <https://doi.org/10.1016/j.ecolmodel.2007.03.041>.
- Bose AK, Weiskittel A, Kuehne C. et al. Does commercial thinning improve stand-level growth of the three most commercially important softwood forest types in North America? *For Ecol Manage* 2018;**409**:683–93. <https://doi.org/10.1016/j.foreco.2017.12.008>.
- Bunn AG. A dendrochronology program library in R (dplR). *Dendrochronologia* 2008;**26**:115–24. <https://doi.org/10.1016/j.dendro.2008.01.002>.
- Burnham KP, Anderson DR, Anderson DR. *Model Selection and Multi-model Inference: A Practical Information-Theoretic Approach*. 2. ed., [4. printing] edition. New York, NY: Springer, 2010.
- Cameron AD. Importance of early selective thinning in the development of long-term stand stability and improved log quality: a review. *Forestry* 2002;**75**:25–35. <https://doi.org/10.1093/forestry/75.1.25>.

- Chadwick AJ, Goodbody TRH, Coops NC. et al. Automatic delineation and height measurement of regenerating conifer crowns under leaf-off conditions using UAV imagery. *Remote Sens (Basel)* 2020;**12**:4104. <https://doi.org/10.3390/rs12244104>.
- Chehreh B, Moutinho A, Viegas C. Latest trends on tree classification and segmentation using UAV data—a review of agroforestry applications. *Remote Sens (Basel)* 2023;**15**:2263. <https://doi.org/10.3390/rs15092263>.
- Contreras MA, Affleck D, Chung W. Evaluating tree competition indices as predictors of basal area increment in western Montana forests. *For Ecol Manage* 2011;**262**:1939–49. <https://doi.org/10.1016/j.foreco.2011.08.031>.
- D'Amato AW, Woodall CW, Weiskittel AR. et al. Carbon conundrums: do United States' current carbon market baselines represent an undesirable ecological threshold? *Glob Chang Biol* 2022;**28**:3991–4. <https://doi.org/10.1111/gcb.16215>.
- Duffy JP, Anderson K, Fawcett D. et al. Drones provide spatial and volumetric data to deliver new insights into microclimate modelling. *Landsc Ecol* 2021;**36**:685–702. <https://doi.org/10.1007/s10980-020-01180-9>.
- Fassnacht FE, Latifi H, Stereńczak K. et al. Review of studies on tree species classification from remotely sensed data. *Remote Sens Environ* 2016;**186**:64–87. <https://doi.org/10.1016/j.rse.2016.08.013>.
- Fassnacht FE, White JC, Wulder MA. et al. Remote sensing in forestry: current challenges, considerations and directions. *Forestry* 2023;**97**:11–37. <https://doi.org/10.1093/forestry/cpad024>.
- Fernández-Sarriá A, Martínez L, Velázquez-Martí B. et al. Different methodologies for calculating crown volumes of *Platanus hispanica* trees using terrestrial laser scanner and a comparison with classical dendrometric measurements. *Comput Electron Agric* 2013;**90**:176–85. <https://doi.org/10.1016/j.compag.2012.09.017>.
- Filipescu CN, Comeau PG. Aspen competition affects light and white spruce growth across several boreal sites in western Canada. *Can J For Res* 2007;**37**:1701–13. <https://doi.org/10.1139/X07-011>.
- García O. Siplab, a spatial individual-based plant modelling system. *Computational Ecology and Software* 2014;**4**:215–22.
- Gavilán-Acuña G, Coops NC, Tompalski P. et al. Estimating potential tree height in *Pinus radiata* plantations using airborne laser scanning data. *Can J For Res* 2022;**52**:1353–66. <https://doi.org/10.1139/cjfr-2022-0121>.
- Goodbody TRH, Coops NC, Hermsilla T. et al. Assessing the status of forest regeneration using digital aerial photogrammetry and unmanned aerial systems. *Int J Remote Sens* 2018;**39**:5246–64. <https://doi.org/10.1080/01431161.2017.1402387>.
- Griess VC, Man CD, Polinko AD. et al. Mitigating midterm timber supply shortage using commercial thinning operations. A case study from British Columbia, Canada. *For Ecol Manage* 2019;**443**:1–18. <https://doi.org/10.1016/j.foreco.2019.04.003>.
- Grubinger S, Coops NC, O'Neill GA. Picturing local adaptation: spectral and structural traits from drone remote sensing reveal clinal responses to climate transfer in common-garden trials of interior spruce (*Picea engelmannii* × *glauca*). *Glob Chang Biol* 2023;**29**:4842–60. <https://doi.org/10.1111/gcb.16855>.
- Gspaltl M, Bauerle W, Binkley D. et al. Leaf area and light use efficiency patterns of Norway spruce under different thinning regimes and age classes. *For Ecol Manage* 2013;**288**:49–59. <https://doi.org/10.1016/j.foreco.2011.11.044>.
- Gülci N, Akay AE, Erdaş O. et al. Planning optimum logging operations through precision forestry approaches. *Eur J Forest Eng* 2015;**1**:56–60.
- Hamraz H, Contreras MA, Zhang J. Forest understory trees can be segmented accurately within sufficiently dense airborne laser scanning point clouds. *Sci Rep* 2017;**7**:6770. <https://doi.org/10.1038/s41598-017-07200-0>.
- Hauglin M, Hansen EH, Næsset E. et al. Accurate single-tree positions from a harvester: a test of two global satellite-based positioning systems. *Scand J For Res* 2017;**32**:774–81. <https://doi.org/10.1080/02827581.2017.1296967>.
- Heygi F. A simulation model for managing jack-pine stands. *Growth Models for Tree and Stand Simulation*. Stockholm, Sweden: Royal College of Forestry, 1974;74–90.
- Jakubowski M, Li W, Guo Q. et al. Delineating individual trees from Lidar data: a comparison of vector- and raster-based segmentation approaches. *Remote Sens (Basel)* 2013;**5**:4163–86. <https://doi.org/10.3390/rs5094163>.
- Jennwein JS, Eitel JUH, Joly K. et al. Estimating integrated measures of forage quality for herbivores by fusing optical and structural remote sensing data. *Environ Res Lett* 2021;**16**:075006. <https://doi.org/10.1088/1748-9326/ac09af>.
- Ke Y, Quackenbush LJ. A review of methods for automatic individual tree-crown detection and delineation from passive remote sensing. *Int J Remote Sens* 2011;**32**:4725–47. <https://doi.org/10.1080/01431161.2010.494184>.
- Keefe RF, Zimbelman EG, Picchi G. Use of individual tree and product level data to improve operational forestry. *Curr For Rep* 2022;**8**:148–65. <https://doi.org/10.1007/s40725-022-00160-3>.
- Lafarge T, Pateiro-López B, Possolo A. et al. R Implementation of a Polyhedral Approximation to a 3D Set of Points Using the α -Shape. *Journal of Statistical Software* 2014;**56**:1–19. <https://doi.org/10.18637/jss.v056.i04>.
- Lämås, T. 2010, The Haglöf PosTex ultrasound instrument for the positioning of objects on forest sample plots. Swedish University of Agricultural Sciences, Department of Forest Resource Management. https://pub.epsilon.slu.se/5461/1/Lamas_t_101019.pdf.
- Leckie DG, Gougeon F, McQueen R. et al. Production of a large-area individual tree species map for forest inventory in a complex forest setting and lessons learned. *Can J Remote Sens* 2017;**43**:140–67. <https://doi.org/10.1080/07038992.2017.1286974>.
- Li W, Guo Q, Jakubowski MK. et al. A new method for segmenting individual trees from the Lidar point cloud. *Photogramm Eng Remote Sensing* 2012;**78**:75–84. <https://doi.org/10.14358/PERS.78.1.75>.
- Lindsay JB. The Whitebox geospatial analysis tools project and open-access GIS. In *Proceedings of the GIS research UK 22nd annual conference, The University of Glasgow* 2014;16–18.
- Lorimer CG. Tests of age-independent competition indices for individual trees in natural hardwood stands. *For Ecol Manage* 1983;**6**:343–60. [https://doi.org/10.1016/0378-1127\(83\)90042-7](https://doi.org/10.1016/0378-1127(83)90042-7).
- Maxwell RS, Larsson L-A. Measuring tree-ring widths using the CooRecorder software application. *Dendrochronologia* 2021;**67**:125841. <https://doi.org/10.1016/j.dendro.2021.125841>.
- Metz J, Seidel D, Schall P. et al. Crown modeling by terrestrial laser scanning as an approach to assess the effect of aboveground intra- and interspecific competition on tree growth. *For Ecol Manage* 2013;**310**:275–88. <https://doi.org/10.1016/j.foreco.2013.08.014>.
- Mohamedou C, Korhonen L, Eerikäinen K. et al. Using LiDAR-modified topographic wetness index, terrain attributes with leaf area index to improve a single-tree growth model in south-eastern Finland. *Forestry* 2019;**92**:253–63. <https://doi.org/10.1093/forestry/cpz010>.
- Moreau G, Chagnon C, Achim A. et al. Opportunities and limitations of thinning to increase resistance and resilience of trees and forests to global change. *Forestry* 2022;**59**:595–615. <https://doi.org/10.1093/forestry/cpac010>.
- Morgan-Wall, T. 2023. Rayshader: create maps and visualize data in 2D and 3D. <https://www.rayshader.com>.

- Pavel M, Byrne K, Gaudreau J-P. et al. Operational manual for commercial thinning in British Columbia. *FPInnovations Research Report* 2021;1–26.
- Persson M, Trubins R, Eriksson LO. et al. Precision thinning – a comparison of optimal stand-level and pixel-level thinning. *Scand J For Res* 2022;**37**:99–108. <https://doi.org/10.1080/02827581.2022.2044902>.
- Pinheiro JC, Bates DM. *Mixed-Effects Models in S and S-PLUS*. 1st edition. New York: SpringerLINK eBooks, 2000.
- Pinno BD, Hossain KL, Gooding T. et al. Opportunities and challenges for intensive silviculture in Alberta, Canada. *Forests* 2021a;**12**:791. <https://doi.org/10.3390/f12060791>.
- Pinno BD, Thomas BR, Liefers VJ. Wood supply challenges in Alberta – growing more timber is the only sustainable solution. *For Chron* 2021b;**97**:106–8. <https://doi.org/10.5558/tfc2021-013>.
- Pretzsch H. Density and growth of forest stands revisited. Effect of the temporal scale of observation, site quality, and thinning. *For Ecol Manage* 2020;**460**:117879. <https://doi.org/10.1016/j.foreco.2020.117879>.
- Pretzsch H. Tree growth as affected by stem and crown structure. *Trees* 2021;**35**:94–60. <https://doi.org/10.1007/s00468-021-02092-0>.
- Pretzsch H, Ahmed S, Jacobs M. et al. Linking crown structure with tree ring pattern: methodological considerations and proof of concept. *Trees* 2022;**36**:1349–67. <https://doi.org/10.1007/s00468-022-02297-x>.
- Pretzsch H, Schütze G. Transgressive overyielding in mixed compared with pure stands of Norway spruce and European beech in Central Europe: evidence on stand level and explanation on individual tree level. *Eur J For Res* 2009;**128**:183–204. <https://doi.org/10.1007/s10342-008-0215-9>.
- Queinnec M, Coops NC, White JC. et al. Mapping dominant boreal tree species groups by combining area-based and individual tree crown LiDAR metrics with Sentinel-2 data. *Can J Remote Sens* 2023;**49**:2130742. <https://doi.org/10.1080/07038992.2022.2130742>.
- Riofrío J, Del Río M, Maguire D. et al. Species mixing effects on height–diameter and basal area increment models for scots pine and maritime pine. *Forests* 2019;**10**:249. <https://doi.org/10.3390/f10030249>.
- Ronoud G, Poorazimy M, Yrttimaa T. et al. Terrestrial laser scanning in assessing the effect of different thinning treatments on the competition of scots pine (*Pinus sylvestris* L.) forests. *Remote Sens (Basel)* 2022;**14**:5196. <https://doi.org/10.3390/rs14205196>.
- Roussel J-R, Auty D, Coops NC. et al. lidR: an R package for analysis of airborne laser scanning (ALS) data. *Remote Sens Environ* 2020;**251**:112061. <https://doi.org/10.1016/j.rse.2020.112061>.
- Seidel D, Hoffmann N, Ehbrecht M. et al. How neighborhood affects tree diameter increment – new insights from terrestrial laser scanning and some methodical considerations. *For Ecol Manage* 2015;**336**:119–28. <https://doi.org/10.1016/j.foreco.2014.10.020>.
- Sørensen R, Zinko U, Seibert J. On the calculation of the topographic wetness index: evaluation of different methods based on field observations. *Hydrol Earth Syst Sci* 2006;**10**:101–12. <https://doi.org/10.5194/hess-10-101-2006>.
- Thieurmél B. Package “Suncalc”: Compute Sun Position, Sunlight Phases, Moon Position and Lunar Phase, 2019; <https://cran.microsoft.com/snapshot/2020-04-20/web/packages/suncalc/suncalc.pdf>.
- Thurm EA, Pretzsch H. Growth–density relationship in mixed stands – results from long-term experimental plots. *For Ecol Manage* 2021;**483**:118909. <https://doi.org/10.1016/j.foreco.2020.118909>.
- Tompalski P, Coops NC, White JC. et al. Estimating changes in Forest attributes and enhancing growth projections: a review of existing approaches and future directions using airborne 3D point cloud data. *Curr For Rep* 2021;**7**:1–24. <https://doi.org/10.1007/s40725-021-00135-w>.
- Weiskittel, AR, Hann DW, Kershaw JA. et al. (Ed.). *Forest Growth and Yield Modeling*. Chichester, UK: John Wiley & Sons, Ltd., 2011. <https://doi.org/10.1002/9781119998518>.
- Wilhelmsson P, Sjödin E, Wästlund A. et al. Dynamic treatment units in forest planning using cell proximity. *Can J For Res* 2021;**51**:1065–71. <https://doi.org/10.1139/cjfr-2020-0210>.
- Wing BM, Boston K, Boston K. et al. A technique for implementing group selection treatments with multiple objectives using an airborne lidar-derived stem map in a heuristic environment. *For Sci* 2019;**65**:211–22. <https://doi.org/10.1093/forsci/fxy050>.
- Wulder M, Niemann KO, Goodenough DG. Local maximum filtering for the extraction of tree locations and basal area from high spatial resolution imagery. *Remote Sens Environ* 2000;**73**:103–14. [https://doi.org/10.1016/S0034-4257\(00\)00101-2](https://doi.org/10.1016/S0034-4257(00)00101-2).
- Yrttimaa T, Luoma V, Saarinen N. et al. Exploring tree growth allometry using two-date terrestrial laser scanning. *For Ecol Manage* 2022;**518**:120303. <https://doi.org/10.1016/j.foreco.2022.120303>.
- Zeide B. Thinning and growth: a full turnaround. *J For* 2001;**99**:20–5. <https://doi.org/10.1093/jof/99.1.20>.
- Zhang W, Qi J, Wan P. et al. An easy-to-use airborne LiDAR data filtering method based on cloth simulation. *Remote Sens (Basel)* 2016;**8**:501. <https://doi.org/10.3390/rs8060501>.
- Zhao D, Borders B, Wilson M. et al. Modeling neighborhood effects on the growth and survival of individual trees in a natural temperate species-rich forest. *Ecol Model* 2006;**196**:90–102. <https://doi.org/10.1016/j.ecolmodel.2006.02.002>.
- Zhu Z, Kleinn C, Nölke N. Assessing tree crown volume—a review. *Forestry* 2021;**94**:18–35. <https://doi.org/10.1093/forestry/cpaa037>.